

Tunable Weyl Points in Periodically Driven Nodal Line Semimetals

Zhongbo Yan^{1,*} and Zhong Wang^{1,2,†}

¹ Institute for Advanced Study, Tsinghua University, Beijing, 100084, China

² Collaborative Innovation Center of Quantum Matter, Beijing 100871, China

Weyl semimetals and nodal line semimetals are characterized by linear band touching at zero-dimensional points and one-dimensional lines, respectively. We predict that a circularly polarized light drives nodal line semimetals into Weyl semimetals. The Floquet Weyl points thus obtained are tunable by the incident light, which enables investigations of them in a highly controllable manner. The transition from nodal line semimetals to Weyl semimetals is accompanied by the emergence of a large and tunable anomalous Hall conductivity. Our predictions are experimentally testable by transport measurement in film samples or by pump-probe angle-resolved photoemission spectroscopy.

PACS numbers: 73.43.-f, 71.70.Ej, 75.70.Tj

It has become well known that topological concepts underlie many fascinating phenomena in condensed matter physics. After in-depth investigations of topological insulators[1–3], considerable attention is now focused on topological semimetals. Unlike topological insulators, whose gapless excitations always live at the sample boundary, topological semimetals host gapless fermions in the bulk. The two major classes of topological semimetals under intense study are (i) nodal point semimetals and (ii) nodal line semimetals (NLSM). The nodal point semimetals include Dirac semimetals(DSM)[4–14] and Weyl semimetals(WSM)[15–31]. The main feature of the band structures of DSMs and WSMs is the linear band-touching points (“Dirac points” and “Weyl points”), which are responsible for most of their interesting properties, including novel phenomena induced by the chiral anomaly[32–44]. NLSMs[45–63] differ in that they contain band-touching *lines* or *rings*[107], away from which the dispersion is linear.

In this Letter we show that driving NLSMs by a circularly polarized light (CPL) creates WSMs, namely, nodal lines become nodal points under radiations. Our work was motivated by recent progress in Floquet topological states [64–83], in particular, Ref.[84] showed that incident light can shift the locations of Weyl points in WSMs. The effect we predict in NLSMs is more dramatic: band-touching lines are driven to points; thus, the dimension of the band-touching manifold is changed. Meanwhile, a large anomalous Hall conductivity tunable by the incident light emerges. Unlike the photoinduced Hall effect in WSMs[84], which is proportional to intensity of incident light, the Hall conductivity in our systems is large and quite insensitive to the light intensity at low temperature, though it depends sensitively on the incident angle of light. The surface Fermi arcs of the Floquet WSMs have a simple interpretation, namely, it comes from tilting the drumhead surface dispersion of NLSMs.

The Floquet WSMs derived from NLSMs are highly tunable, in particular, the Weyl points can be freely tuned to any locations on the nodal line. Hopefully this tunability will motivate further investigations of fascinating properties of topological materials.

Recently, there have appeared experimental evidences of nodal lines in PbTaSe₂[55], ZrSiS[85–88], ZrSiTe[89],

and PtSn₄[90], and quite a few theoretical proposals in Cu₃PdN[53, 54] Ca₃P₂[56, 61] Hg₃As₂[91] and three-dimensional graphene networks[52]. Thus our prediction can be experimentally tested in the near future.

Drive nodal line semimetals to Weyl semimetals.— NLSMs with negligible spin-orbit coupling (SOC) can be regarded as two copies of spinless systems; thus, we first consider spinless models for notational simplicity. Near the nodal line, the physics can be captured by two-band models[53, 54, 59]. Our starting point is the model Hamiltonian $\hat{H} = \sum_{\mathbf{k}} \hat{\Psi}_{\mathbf{k}}^{\dagger} \mathcal{H}(\mathbf{k}) \hat{\Psi}_{\mathbf{k}}$ with $\hat{\Psi}_{\mathbf{k}} = (\hat{c}_{\mathbf{k},a}, \hat{c}_{\mathbf{k},b})^T$ and $(\hbar = c = k_B = 1)$,

$$\mathcal{H}(\mathbf{k}) = [m - Bk^2]\tau_x + vk_z\tau_z + \epsilon_0(\mathbf{k})\tau_0, \quad (1)$$

where a, b refer to the two orbitals involved and m, B are positive constants with the dimension of energy and inverse energy, respectively; v refers to the Fermi velocity along z direction; $k^2 = k_x^2 + k_y^2 + k_z^2$, and $\tau_{x,y,z}$ are Pauli matrices and τ_0 is the identity matrix. Although quite simple, this two-band model well describes several candidates of NLSMs[53, 54] in which the spin-orbit coupling can be neglected. The form of $\epsilon_0(\mathbf{k})$ is not crucial and is specified later. When $\epsilon_0 = 0$, the energy spectra of this Hamiltonian read

$$E_{\pm, \mathbf{k}} = \pm \sqrt{[m - Bk^2]^2 + v^2k_z^2}. \quad (2)$$

The nodal ring, on which the two bands touch, is located at the $k_z = 0$ plane and determined by the equation $k_x^2 + k_y^2 = m/B$. The nodal ring is protected by a mirror symmetry, $\mathcal{M}\mathcal{H}(k_x, y, k_z)\mathcal{M}^{-1} = \mathcal{H}(k_x, y, -k_z)$, with $\mathcal{M} = i\tau_x$ [108].

We study the effects of a periodic driving. For the sake of concreteness, suppose that a light beam comes in the x direction, with the vector potential $\mathbf{A}(t) = A_0[0, \cos(\omega t), \sin(\omega t + \phi)]$ [109]. The choice $\phi = 0$ and $\phi = \pi$ corresponds to right-handed and left-handed circularly polarized light (CPL), respectively. The electromagnetic coupling is given by $\mathcal{H}(\mathbf{k}) \rightarrow \mathcal{H}(\mathbf{k} + e\mathbf{A}(t))$. The full Hamiltonian is time periodic; thus, it can be expanded as $\mathcal{H}(t, \mathbf{k}) = \sum_n \mathcal{H}_n(\mathbf{k})e^{in\omega t}$ with

$$\begin{aligned} \mathcal{H}_0(\mathbf{k}) &= [m - Be^2A_0^2 - Bk^2]\tau_x + vk_z\tau_z, \\ \mathcal{H}_{\pm 1}(\mathbf{k}) &= -eA_0[2B(k_y \mp ie^{\pm i\phi}k_z)\tau_x \pm ie^{\pm i\phi}v\tau_z]/2, \\ \mathcal{H}_{\pm 2}(\mathbf{k}) &= -Be^2A_0^2(1 - e^{\pm i2\phi})\tau_x/4, \end{aligned} \quad (3)$$

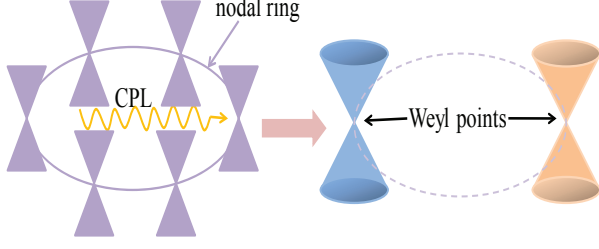


FIG. 1: Conceptual illustration. A Dirac nodal line semimetal has band-touching lines/rings and linear dispersion in the two transverse directions. CPL lifts all the band touching except at two isolated points, near which the dispersion of the Floquet bands is linear in all three directions, i.e., Weyl points. The different colors of the Weyl cones represent different chirality (± 1).

and $\mathcal{H}_n = 0$ for $|n| > 2$. In the limit where the driving frequency ω is large compared to the other energy scales, a proper description of the system is the effective time-independent Hamiltonian[65, 92–95], which reads

$$\begin{aligned} \mathcal{H}_{\text{eff}}(\mathbf{k}) &= \mathcal{H}_0 + \sum_{n \geq 1} \frac{[\mathcal{H}_{+n}, \mathcal{H}_{-n}]}{n\omega} + \mathcal{O}\left(\frac{1}{\omega^2}\right) \\ &= [\tilde{m} - Bk^2]\tau_x + vk_z\tau_z + \lambda k_y\tau_y + \dots, \end{aligned} \quad (4)$$

where $\lambda = -2e^2 BvA_0^2 \cos \phi / \omega$ and $\tilde{m} = m - Be^2 A_0^2$. The main effect of the driving manifests in the $\lambda k_y\tau_y$ term, which is nonzero as long as $\cos \phi \neq 0$, though circular polarizations ($\phi = 0$ or π) maximize $|\lambda|$. The energy spectra of \mathcal{H}_{eff} are given by

$$\tilde{E}_{\pm, \mathbf{k}} = \pm \sqrt{[\tilde{m} - Bk^2]^2 + v^2 k_z^2 + (\lambda k_y)^2}. \quad (5)$$

Once $\lambda \neq 0$, the energy spectra immediately become gapped except at the two Weyl points $\mathbf{K}_{\pm} = \pm(\sqrt{\tilde{m}/B}, 0, 0)$ (see Fig.1). We can expand \mathcal{H}_{eff} around the Weyl points as $\mathcal{H}_{\pm}(\mathbf{q}) = \sum_{ij} v_{ij} q_i \tau_j$ with $\mathbf{q} = \mathbf{k} - \mathbf{K}_{\pm}$ referring to the momentum relative to the gapless points, with $v_{xx} = \mp 2\sqrt{\tilde{m}B}$, $v_{yy} = \lambda$, $v_{zz} = v$, and all other matrix entries are 0. The chirality of the Weyl points at \mathbf{K}_{\pm} is $\chi_{\pm} \equiv \text{sgn}[\det(v_{ij})] = \pm \text{sgn}(\cos \phi)$. The appearance of $\cos \phi$ implies that the chirality has a simple dependence on the handedness of the incident laser beam; thus, reversing the handedness causes the reversing of the chirality of Weyl points. Moreover, the locations of the Weyl points are tunable by changing the direction of the incident laser beams. For instance, the two Weyl points are located at $\pm(0, \sqrt{\tilde{m}/B}, 0)$ if the laser beam is along the y direction.

If one considers a nodal ring of generic shape and the incident light along the x direction, one can show that Weyl points are created around the local maxima and local minima of k_x on the nodal ring, and the chirality of the Weyl point is opposite on the maxima and minima. Since the numbers of local minima and local maxima are equal on a ring, the Nielsen-Ninomiya theorem[96] stating the equality of the numbers of Weyl points with opposite chirality is automatically satisfied.

Anomalous Hall effect (AHE).— One of the significant consequences of the topological transition from NLSM to WSM is the emergence of the AHE characterized by a nonzero Hall conductivity. The conductivity can be obtained from the linear response theory[66], which leads to

$$\sigma_{\mu\nu} = e^2 \epsilon_{\mu\nu\rho} \int \frac{d^3k}{(2\pi)^3} \sum_{\alpha} f_{\alpha}(k) [\nabla_{\mathbf{k}} \times \mathcal{A}_{\alpha}(\mathbf{k})]_{\rho} \quad (6)$$

where $\mu, \nu, \rho = x, y, z$ and $\epsilon_{\mu\nu\rho} = \pm 1$ for the even (odd) permutation of (x, y, z) , $\alpha \equiv (i, n)$, with i referring to the original band index and n referring to the Floquet index[66]; $\mathcal{A}_{\alpha}(\mathbf{k})$ is the Berry connection, and f_{α} is the occupation function. Thus the Hall conductivity depends not only on the Berry curvature but also on the fermion occupation, the latter of which is nonuniversal, being dependent on details of the systems (e.g. the coupling between the systems and the bath). Below we focus on the case in which the occupation is close to equilibrium, namely, $f_{(i,n)} = \delta_{n0} n_i(E_{i,\mathbf{k}})$, where $n_i(E_{i,\mathbf{k}})$ is the Fermi-Dirac distribution. For the incident light beams along the x direction, the interesting component of the Hall conductivity is σ_{yz} , which can be found as (Supplemental Material)

$$\begin{aligned} \sigma_{yz}(T, \mu, \lambda) &= \frac{e^2}{2} \int \frac{d^3k}{(2\pi)^3} [\hat{\mathbf{d}} \cdot (\frac{\partial \hat{\mathbf{d}}}{\partial k_y} \times \frac{\partial \hat{\mathbf{d}}}{\partial k_z})] (n_{+} - n_{-}) \\ &= \frac{e^2}{2} \int \frac{d^3k}{(2\pi)^3} \frac{\lambda v (\tilde{m} - 2Bk_x^2 + Bk^2)}{\tilde{E}_{+,\mathbf{k}}^3} (n_{+} - n_{-}) \end{aligned} \quad (7)$$

where $\hat{\mathbf{d}} = \mathbf{d}/|\mathbf{d}|$ with $\mathbf{d} = \text{Tr}[\nabla_{\mathbf{k}} \mathcal{H}_{\text{eff}}]/2$, and $n_{\pm} = 1/[e^{(\tilde{E}_{\pm,\mathbf{k}} - \mu)/T} + 1]$ is the Fermi-Dirac distribution with μ denoting the chemical potential. For nonzero temperature ($T \neq 0$) or doped system ($\mu \neq 0$), analytic simplification of Eq.(7) is not available, and we need to treat Eq.(7) numerically (see Fig.2). From Fig.2(a) we can see that $\sigma_{yz}(T, 0, \lambda)$ increases and saturates as λ is increased. The saturation occurs at smaller λ when T is lower. As $T \rightarrow 0$, the σ_{yz} - λ curve approaches a step function, jumping from $\sigma_{yz} = 0$ at $\lambda = 0$ to a nonzero value $\sigma_{yz}(0, 0, \lambda \neq 0)$ at $\lambda > 0$. Taking $\mu = T = 0$ in Eq.(7) leads to

$$\sigma_{yz}(0, 0, \lambda \neq 0) = \frac{e^2}{\pi h} \sqrt{\frac{m}{B}} - e^2 A_0^2 \text{sgn}(\cos \phi), \quad (8)$$

where we have restored the Planck constant h . It is readily seen that $\sigma_{yz}(0, 0, \lambda \neq 0)$ is proportional to the distance between the two Weyl points. The Hall conductivity can be easily tuned by the incident angle of light. For instance, the nonzero component is σ_{xz} instead of σ_{yz} if the incident light is along the y direction.

This behavior is remarkably different from the light-induced Hall effect in Weyl semimetals[84]. The proposal of Ref.[84] is to separate existing Weyl points in WSMs by light, while ours is to create Weyl points from NLSMs. The former is a second-order effect proportional to A_0^2 , while the AHE in the present work is a zeroth-order effect, which should be much more pronounced in experiment. In general, the dis-

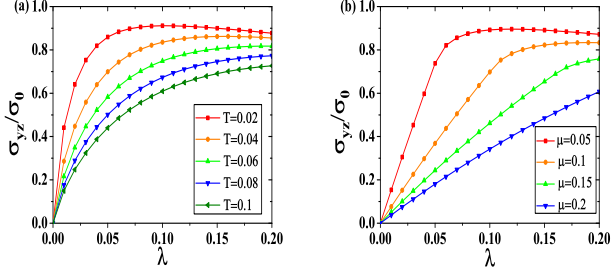


FIG. 2: The dependence of Hall conductivity on temperature (T), chemical potential (μ), and the intensity of the incident light beam λ . The common parameters in use are $m = 1$, $B = 1$, $\omega = 2$, $\phi = \pi$, $v = 1$, $\epsilon_0 = 0$, and we have defined the shorthand notation $\sigma_0 = \frac{e^2}{\pi h} \sqrt{\frac{m}{B}}$. (a) σ_{yz} at $\mu = 0$ as a function of λ for several values of T ; (b) σ_{yz} at $T = 0$ as a function of λ for several values of μ .

tance between the two photoinduced Weyl points is of the order of $2\pi/a$, a referring to the lattice constant; thus, we have the estimation $\sigma_{yz} \sim (e^2/h)(2\pi/a)$.

Fermi arc as the descendent of drumhead states.— The dispersion of the surface states of the NLSM takes the shape of a drumhead or a bowl, i.e., a nearly flat band bounded by the projection of the bulk nodal line to the surface Brillouin zone. When $\epsilon_0 = 0$, the dispersion becomes exactly flat. Since the NLSM is driven to a WSM phase in our study, it is a natural question how a Fermi arc comes from a drumhead (or bowl). We consider a semi-infinite geometry, namely, the sample occupies the entire $z > 0$ half-space. The \mathbf{k} -space energy eigenvalue problem is translated to the real space as $\mathcal{H}_{\text{eff}}(k_x, k_y, -i\partial_z)\Psi(x, y, z) = E(k_x, k_y)\Psi(x, y, z)$, under the boundary conditions $\Psi(z = 0) = 0$ and $\Psi(z \rightarrow +\infty) = 0$.

We find that the surface mode wave function takes the form of

$$\Psi(x, y, z) = \mathcal{N} e^{ik_x x} e^{ik_y y} \sin(\kappa z) e^{-\gamma z} \chi, \quad (9)$$

with

$$E(k_x, k_y) = -\lambda k_y + \epsilon_0(k_x, k_y), \quad (10)$$

where $\chi = (1, -i)^T / \sqrt{2}$, \mathcal{N} is a normalization factor, and $\gamma = \frac{v}{2B}$, $\kappa = \frac{1}{2B} \sqrt{4B[\tilde{m} - B(k_x^2 + k_y^2)] - v^2}$. Implicit here is that $4B[\tilde{m} - B(k_x^2 + k_y^2)] - v^2 > 0$, so that κ is real valued; in the cases of $4B[\tilde{m} - B(k_x^2 + k_y^2)] - v^2 < 0$, the solution can be obtained by replacing $\sin(\kappa z)$ by $\sinh(|\kappa|z)$, namely, $\Psi(x, y, z) = \mathcal{N} e^{ik_x x} e^{ik_y y} \sinh(|\kappa|z) e^{-\gamma z} \chi$. It is found that the normalizability requires

$$k_x^2 + k_y^2 < \tilde{m}/B, \quad (11)$$

which determines the region where the surface modes exist. It is notable that the dispersion given by Eq.(10) shows a chiral nature in the y direction. As a comparison, we note that the surface states of the NLSM can be recovered by letting $\lambda = 0$, which, according to Eq.(10), leads to the dispersion

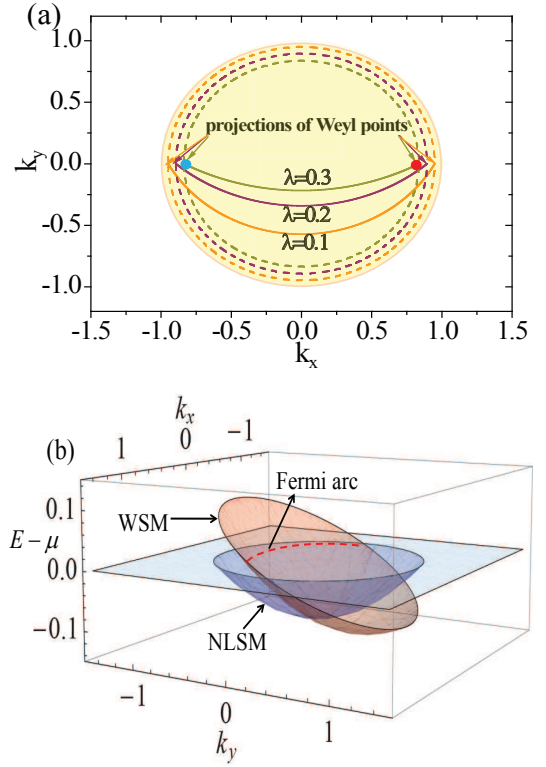


FIG. 3: The surface states of the NLSM and the Floquet WSM. The values of parameters are taken to be $m = B = 1$, $\omega = 2$, $\phi = \pi$, $v = 1$, and $\epsilon_0(k) = 0.1(k_x^2 + k_y^2)$. The chemical potential μ has been tuned to the Weyl band-touching points. (a) The shadow area ($k_x^2 + k_y^2 < m/B$) represents the drumhead surface states of the pristine NLSM, and the dashed lines enclose the area of surface states of the Floquet WSM ($k_x^2 + k_y^2 < \tilde{m}/B$), with the three colors referring to three values of λ , as indicated in the figure. The solid curves are the Fermi arcs connecting the projections of the two Weyl points onto the surface Brillouin zone. (b) The surface state dispersions of both the pristine NLSM and the Floquet WSM (with the driving parameter $\lambda = 0.1$). Tilting the surface state dispersion of the NLSM leads to that of the WSM. The intersection of the dispersion of WSM and the $E = \mu$ plane is the Fermi arc.

of the drumhead or bowl states: $E(k_x, k_y) = \epsilon_0(k_x, k_y)$. The region of the drumhead or bowl is given by Eq.(11) with \tilde{m} replaced by m , namely, $k_x^2 + k_y^2 < m/B$. An illustration is given in Fig.3(a), in which the surface state of the pristine NLSM is represented by the shadow area, and the surface states of the Floquet WSM for three values of intensity of incident laser are enclosed by the three dashed lines with different colors. Because of the nonzero λ generated by the incident laser, which enters Eq.(10), the dispersion of the drumhead or bowl states of the pristine NLSM becomes tilted (see Fig.3(b)).

Spinful NLSMs.— SOC can change the size and location of nodal lines or gap them out. Let us first consider the first case. For concreteness, we consider a model Hamiltonian $\mathcal{H}_s(\mathbf{k}) = (m - Bk^2)\tau_x + vk_z\tau_z + \Delta_{\text{so}}\tau_x s_z$, where s_z is the Pauli matrix for spin, and Δ_{so} quantifies SOC. This model hosts two nodal lines, and is relevant to the NLSM candi-

date TlTaSe₂[60]. Using the method of the previous sections, we can find the effective Floquet Hamiltonian $\mathcal{H}_{s,\text{eff}}(\mathbf{k}) = (m - Bk^2)\tau_x + vk_z\tau_z + \Delta_{\text{so}}\tau_x s_z + \lambda k_y\tau_y$, with spectrum $E = \pm \sqrt{(\tilde{m} \pm \Delta_{\text{so}} - Bk^2)^2 + v^2 k_z^2 + \lambda^2 k_y^2}$, in which the expressions for λ and \tilde{m} are the same as given below Eq.(4). Thus the system is driven to the WSM phase with four Weyl points at $\mathbf{K}_1^\pm = \pm(\sqrt{(\tilde{m} + \Delta_{\text{so}})/B}, 0, 0)$ and $\mathbf{K}_2^\pm = \pm(\sqrt{(\tilde{m} - \Delta_{\text{so}})/B}, 0, 0)$.

Effect of a small gap.— In several candidates of NLSMs, the nodal line can be gapped out if a small spin-orbit coupling[53, 54, 91] is included. Below we show that such a small gap introduces a threshold laser intensity. Let us consider the model

$$\mathcal{H}_g(\mathbf{k}) = (m - Bk^2)\tau_x + vk_z\tau_z + \lambda_{\text{so}}\tau_y s_z, \quad (12)$$

where s_z refers to the z component of spin, and the $\lambda_{\text{so}}\tau_y s_z$ term induces an energy gap $2|\lambda_{\text{so}}|$. With an incident laser, the effective Hamiltonian reads

$$\mathcal{H}_{g,\text{eff}}(\mathbf{k}) = (m - Bk^2)\tau_x + vk_z\tau_z + \lambda_{\text{so}}\tau_y s_z + \lambda k_y\tau_y, \quad (13)$$

with spectrum $E = \pm \sqrt{(\tilde{m} - Bk^2)^2 + v^2 k_z^2 + (\lambda k_y \pm \lambda_{\text{so}})^2}$. There are clearly four generated Weyl points, located at $\mathbf{Q}_1^\pm = (\pm \sqrt{\tilde{m}/B - (\lambda_{\text{so}}/\lambda)^2}, \lambda_{\text{so}}/\lambda, 0)$, and $\mathbf{Q}_2^\pm = (\pm \sqrt{\tilde{m}/B - (\lambda_{\text{so}}/\lambda)^2}, -\lambda_{\text{so}}/\lambda, 0)$. It is readily seen that the main effect of the gap is a threshold laser intensity $\lambda_{\text{th}} = \sqrt{\lambda_{\text{so}}^2 B/\tilde{m}}$, above which the Weyl points can be generated. Below the threshold laser intensity the system is gapped.

Experimental considerations.— Among other possibilities, it should be feasible to test our predictions in the film of NLSMs. The incident light has a finite penetration depth δ , and it is most efficient to measure the Hall conductivity in film with thickness $\sim \delta$. The estimation of δ becomes simple when the Fermi velocities along the z direction and the $x - y$ direction are the same, namely, when $2\sqrt{mB} = v$, and the optical absorption rate can be straightforwardly estimated following Ref.[97], leading to $\delta \sim \sqrt{B/(m\alpha^2)}$, where $\alpha \sim 1/137$ is the fine structure constant. Since $\sqrt{B/m}$ is the inverse of the radius of the nodal ring, we expect that it is of the order of a few lattice constants, thus $\delta \sim$ several hundred lattice constants. Taking the NLSM candidate ZrSiS as an example, we have estimated that a film of thickness 100nm and size $100\mu\text{m} \times 100\mu\text{m}$ can generate a Hall voltage ~ 1 mV with a dc current of 100 mA (Supplemental Material), which can be readily measured experimentally.

In the pump-probe experiments[78], $2e^2 v^2 A_0^2/\omega \sim 50\text{meV}$ is attainable at photon energy $\hbar\omega = 120\text{meV}$ (Ref.[78]); therefore, if we take $v^2/B \sim 0.5\text{eV}$, we have $|\lambda| \sim 0.1v$. Since we have shown that the Fermi velocity of the Fermi arc is λ , we can see that, within the current experimental feasibility, it can reach a tenth of the bulk Fermi velocity of the NLSMs. This can be detected by the pump-probe angle-resolved photoemission spectroscopy (ARPES)[78, 79].

Conclusions.— We have shown that NLSMs are tailor-made materials for optically creating Floquet Weyl points.

Remarkably, polarized light with infinitesimal intensity is sufficient in principle. The resultant Floquet WSMs have a large AHE controllable by the laser beams, e.g., reversing the handedness of the incident light changes the sign of the anomalous Hall conductivity. The Fermi arcs of the Floquet WSMs have an appealing interpretation, namely, they come from tilting the drumhead surface dispersion of NLSMs. The photoinduced Fermi arcs and bulk Weyl points can be detected in pump-probe ARPES, and the AHE can be measured in transport experiments. Our proposal can be generalized to cold-atom systems[98] by shaking lattice[99–101].

Apart from potential applications of the large and tunable AHE in high-speed electronics, the tunability of the Floquet WSMs also facilitates the future investigations of many novel physics therein by techniques absent in the static systems (e.g. spatial modulation of light [102]). From a broader perspective, our work suggests that Floquet topological semimetals are fruitful platforms in the study of topological matters.

Acknowledgements. This work is supported by NSFC under Grant No. 11304175.

Note added: After initial submission of this letter, there appeared two related preprints[103, 104]. In the overlapping parts, their conclusions are consistent with ours.

* yzhbo@mail.tsinghua.edu.cn

† wangzhongemail@tsinghua.edu.cn

- [1] M. Z. Hasan and C. L. Kane, Rev. Mod. Phys. **82**, 3045 (2010).
- [2] X.-L. Qi and S.-C. Zhang, Rev. Mod. Phys. **83**, 1057 (2011).
- [3] C.-K. Chiu, J. C. Y. Teo, A. P. Schnyder, and S. Ryu, ArXiv e-prints (2015), 1505.03535.
- [4] Z. Liu, B. Zhou, Y. Zhang, Z. Wang, H. Weng, D. Prabhakaran, S.-K. Mo, Z. Shen, Z. Fang, X. Dai, et al., Science **343**, 864 (2014).
- [5] M. Neupane, S.-Y. Xu, R. Sankar, N. Alidoust, G. Bian, C. Liu, I. Belopolski, T.-R. Chang, H.-T. Jeng, H. Lin, et al., Nat. Commun. **5**, 3786 (2014), 1309.7892.
- [6] S. Borisenko, Q. Gibson, D. Evtushinsky, V. Zabolotnyy, B. Büchner, and R. J. Cava, Phys. Rev. Lett. **113**, 027603 (2014).
- [7] S.-Y. Xu, C. Liu, S. K. Kushwaha, R. Sankar, J. W. Krizan, I. Belopolski, M. Neupane, G. Bian, N. Alidoust, T.-R. Chang, et al., Science **347**, 294 (2015).
- [8] Z. Wang, Y. Sun, X.-Q. Chen, C. Franchini, G. Xu, H. Weng, X. Dai, and Z. Fang, Phys. Rev. B **85**, 195320 (2012).
- [9] S. M. Young, S. Zaheer, J. C. Teo, C. L. Kane, E. J. Mele, and A. M. Rappe, Phys. Rev. Lett. **108**, 140405 (2012).
- [10] Z. Wang, H. Weng, Q. Wu, X. Dai, and Z. Fang, Phys. Rev. B **88**, 125427 (2013).
- [11] A. Sekine and K. Nomura, Phys. Rev. B **90**, 075137 (2014).
- [12] C. Zhang, E. Zhang, Y. Liu, Z.-G. Chen, S. Liang, J. Cao, X. Yuan, L. Tang, Q. Li, T. Gu, et al., ArXiv e-prints (2015), 1504.07698.
- [13] R. Y. Chen, Z. G. Chen, X.-Y. Song, J. A. Schneeloch, G. D. Gu, F. Wang, and N. L. Wang, Phys. Rev. Lett. **115**, 176404 (2015).
- [14] X. Yuan, C. Zhang, Y. Liu, C. Song, S. Shen, X. Sui, J. Xu, H. Yu, Z. An, J. Zhao, et al., ArXiv e-prints (2015),

- 1510.00907.
- [15] X. Wan, A. M. Turner, A. Vishwanath, and S. Y. Savrasov, Phys. Rev. B **83**, 205101 (2011).
- [16] H. B. Nielsen and M. Ninomiya, Phys. Lett. B **130**, 389 (1983).
- [17] G. E. Volovik, *The Universe in a Helium Droplet* (Oxford University Press, USA, 2003).
- [18] K.-Y. Yang, Y.-M. Lu, and Y. Ran, Phys. Rev. B **84**, 075129 (2011).
- [19] A. A. Burkov and L. Balents, Phys. Rev. Lett. **107**, 127205 (2011).
- [20] H. Weng, C. Fang, Z. Fang, B. A. Bernevig, and X. Dai, Phys. Rev. X **5**, 011029 (2015).
- [21] S.-M. Huang, S.-Y. Xu, I. Belopolski, C.-C. Lee, G. Chang, B. Wang, N. Alidoust, G. Bian, M. Neupane, A. Bansil, et al., Nat. Commun. **6**, 7373 (2015).
- [22] C. Zhang, Z. Yuan, S. Xu, Z. Lin, B. Tong, M. Zahid Hasan, J. Wang, C. Zhang, and S. Jia, ArXiv e-prints (2015), 1502.00251.
- [23] S.-Y. Xu, I. Belopolski, N. Alidoust, M. Neupane, G. Bian, C. Zhang, R. Sankar, G. Chang, Z. Yuan, C.-C. Lee, et al., Science **349**, 613 (2015).
- [24] B. Q. Lv, H. M. Weng, B. B. Fu, X. P. Wang, H. Miao, J. Ma, P. Richard, X. C. Huang, L. X. Zhao, G. F. Chen, et al., ArXiv e-prints (2015), 1502.04684.
- [25] X. Huang, L. Zhao, Y. Long, P. Wang, D. Chen, Z. Yang, H. Liang, M. Xue, H. Weng, Z. Fang, et al., Phys. Rev. X **5**, 031023 (2015).
- [26] L. Yang, Z. Liu, Y. Sun, H. Peng, H. Yang, T. Zhang, B. Zhou, Y. Zhang, Y. Guo, M. Rahn, et al., ArXiv e-prints (2015), 1507.00521.
- [27] N. Ghimire, Y. Luo, M. Neupane, D. Williams, E. Bauer, and F. Ronning, J. Phys.: Condens. Matter **27**, 152201 (2015).
- [28] C. Shekhar, A. K. Nayak, Y. Sun, M. Schmidt, M. Nicklas, I. Leermakers, U. Zeitler, Y. Skourski, J. Wosnitza, Z. Liu, et al., Nat. Phys. **11**, 645 (2015).
- [29] S.-Y. Xu, N. Alidoust, I. Belopolski, C. Zhang, G. Bian, T.-R. Chang, H. Zheng, V. Stokov, D. S. Sanchez, G. Chang, et al., ArXiv e-prints (2015), 1504.01350.
- [30] L. Lu, Z. Wang, D. Ye, L. Ran, L. Fu, J. D. Joannopoulos, and M. Soljačić, Science **349**, 622 (2015).
- [31] L. Lu, L. Fu, J. D. Joannopoulos, and M. Soljačić, Nat. Photonics **7**, 294 (2013).
- [32] D. T. Son and B. Z. Spivak, ArXiv e-prints (2012), 1206.1627.
- [33] C.-X. Liu, P. Ye, and X.-L. Qi, Phys. Rev. B **87**, 235306 (2013).
- [34] V. Aji, Phys. Rev. B **85**, 241101 (2012).
- [35] A. A. Zyuzin and A. A. Burkov, ArXiv e-prints (2012), 1206.1868.
- [36] Z. Wang and S.-C. Zhang, Phys. Rev. B **87**, 161107 (2013).
- [37] P. Hosur and X.-L. Qi, Phys. Rev. B **91**, 081106 (2015).
- [38] P. Hosur and X. Qi, Comptes Rendus Physique **14**, 857 (2013), 1309.4464.
- [39] H.-J. Kim, K.-S. Kim, J.-F. Wang, M. Sasaki, N. Satoh, A. Ohnishi, M. Kitaura, M. Yang, and L. Li, Phys. Rev. Lett. **111**, 246603 (2013).
- [40] S. A. Parameswaran, T. Grover, D. A. Abanin, D. A. Pesin, and A. Vishwanath, Phys. Rev. X **4**, 031035 (2014).
- [41] J. Zhou, H.-R. Chang, and D. Xiao, Phys. Rev. B **91**, 035114 (2015).
- [42] Q. Li, D. E. Kharzeev, C. Zhang, Y. Huang, I. Pletikoscic, A. V. Fedorov, R. D. Zhong, J. A. Schneeloch, G. D. Gu, and T. Valla, ArXiv e-prints (2014), 1412.6543.
- [43] R. Bi and Z. Wang, Phys. Rev. B **92**, 241109 (2015).
- [44] P. Goswami, J. H. Pixley, and S. Das Sarma, Phys. Rev. B **92**, 075205 (2015).
- [45] A. A. Burkov, M. D. Hook, and L. Balents, Phys. Rev. B **84**, 235126 (2011).
- [46] J.-M. Carter, V. V. Shankar, M. A. Zeb, and H.-Y. Kee, Phys. Rev. B **85**, 115105 (2012).
- [47] M. Phillips and V. Aji, Phys. Rev. B **90**, 115111 (2014).
- [48] Y. Chen, Y.-M. Lu, and H.-Y. Kee, Nat. Commun. **6**, 6593 (2015).
- [49] M. Zeng, C. Fang, G. Chang, Y.-A. Chen, T. Hsieh, A. Bansil, H. Lin, and L. Fu, ArXiv e-prints (2015), 1504.03492.
- [50] C.-K. Chiu and A. P. Schnyder, Phys. Rev. B **90**, 205136 (2014).
- [51] K. Mullen, B. Uchoa, and D. T. Glatzhofer, Phys. Rev. Lett. **115**, 026403 (2015).
- [52] H. Weng, Y. Liang, Q. Xu, R. Yu, Z. Fang, X. Dai, and Y. Kawazoe, Phys. Rev. B **92**, 045108 (2015).
- [53] R. Yu, H. Weng, Z. Fang, X. Dai, and X. Hu, Phys. Rev. Lett. **115**, 036807 (2015).
- [54] Y. Kim, B. J. Wieder, C. L. Kane, and A. M. Rappe, Phys. Rev. Lett. **115**, 036806 (2015).
- [55] G. Bian, T.-R. Chang, R. Sankar, S.-Y. Xu, H. Zheng, T. Neupert, C.-K. Chiu, S.-M. Huang, G. Chang, I. Belopolski, et al., Nat. Commun. **7**, 10556 (2016).
- [56] L. S. Xie, L. M. Schoop, E. M. Seibel, Q. D. Gibson, W. Xie, and R. J. Cava, APL Mater. **3**, 083602 (2015).
- [57] J.-W. Rhim and Y. B. Kim, Phys. Rev. B **92**, 045126 (2015).
- [58] Y. Chen, Y. Xie, S. A. Yang, H. Pan, F. Zhang, M. L. Cohen, and S. Zhang, ArXiv e-prints (2015), 1505.02284.
- [59] C. Fang, Y. Chen, H.-Y. Kee, and L. Fu, Phys. Rev. B **92**, 081201 (2015).
- [60] G. Bian, T.-R. Chang, H. Zheng, S. Velury, S.-Y. Xu, T. Neupert, C.-K. Chiu, S.-M. Huang, D. S. Sanchez, I. Belopolski, et al., Phys. Rev. B **93**, 121113 (2016).
- [61] Y.-H. Chan, C.-K. Chiu, M. Y. Chou, and A. P. Schnyder, Phys. Rev. B **93**, 205132 (2016).
- [62] J.-W. Rhim and Y. B. Kim, New J. Phys. **18**, 043010 (2016), 1511.07885.
- [63] Z. Yan, P.-W. Huang, and Z. Wang, Phys. Rev. B **93**, 085138 (2016).
- [64] N. H. Lindner, G. Refael, and V. Galitski, Nat. Phys. **7**, 490 (2011).
- [65] T. Kitagawa, T. Oka, A. Brataas, L. Fu, and E. Demler, Phys. Rev. B **84**, 235108 (2011).
- [66] T. Oka and H. Aoki, Phys. Rev. B **79**, 081406 (2009).
- [67] J.-i. Inoue and A. Tanaka, Phys. Rev. Lett. **105**, 017401 (2010).
- [68] Z. Gu, H. A. Fertig, D. P. Arovas, and A. Auerbach, Phys. Rev. Lett. **107**, 216601 (2011).
- [69] T. Kitagawa, M. S. Rudner, E. Berg, and E. Demler, Phys. Rev. A **82**, 033429 (2010).
- [70] T. Kitagawa, E. Berg, M. Rudner, and E. Demler, Phys. Rev. B **82**, 235114 (2010).
- [71] N. H. Lindner, D. L. Bergman, G. Refael, and V. Galitski, Phys. Rev. B **87**, 235131 (2013).
- [72] L. Jiang, T. Kitagawa, J. Alicea, A. R. Akhmerov, D. Pekker, G. Refael, J. I. Cirac, E. Demler, M. D. Lukin, and P. Zoller, Phys. Rev. Lett. **106**, 220402 (2011).
- [73] M. S. Rudner, N. H. Lindner, E. Berg, and M. Levin, Phys. Rev. X **3**, 031005 (2013).
- [74] J. P. Dahlhaus, J. M. Edge, J. Tworzydło, and C. W. J. Beenakker, Phys. Rev. B **84**, 115133 (2011).
- [75] A. Gómez-León and G. Platero, Phys. Rev. Lett. **110**, 200403 (2013).
- [76] Y. Zhou and M. W. Wu, Phys. Rev. B **83**, 245436 (2011).

- [77] P. Delplace, A. Gómez-León, and G. Platero, Phys. Rev. B **88**, 245422 (2013).
- [78] Y. Wang, H. Steinberg, P. Jarillo-Herrero, and N. Gedik, Science **342**, 453 (2013).
- [79] F. Mahmood, C.-K. Chan, Z. Alpichshev, D. Gardner, Y. Lee, P. A. Lee, and N. Gedik, Nat. Phys. **12**, 306 (2016).
- [80] R. Wang, B. Wang, R. Shen, L. Sheng, and D. Xing, Europhys. Lett. **105**, 17004 (2014).
- [81] K. I. Seetharam, C.-E. Bardyn, N. H. Lindner, M. S. Rudner, and G. Refael, Phys. Rev. X **5**, 041050 (2015).
- [82] H. Hübener, M. A. Sentef, U. de Giovannini, A. F. Kemper, and A. Rubio, ArXiv e-prints (2016), 1604.03399.
- [83] H. Wang, L. Zhou, and Y. D. Chong, Phys. Rev. B **93**, 144114 (2016).
- [84] C.-K. Chan, P. A. Lee, K. S. Burch, J. H. Han, and Y. Ran, Phys. Rev. Lett. **116**, 026805 (2016).
- [85] L. M. Schoop, M. N. Ali, C. Straßer, V. Duppl, S. S. Parkin, B. V. Lotsch, and C. R. Ast, arXiv preprint arXiv:1509.00861 (2015).
- [86] M. Neupane, I. Belopolski, M. M. Hosen, D. S. Sanchez, R. Sankar, M. Szlowska, S.-Y. Xu, K. Dimitri, N. Dhakal, P. Maldonado, et al., Phys. Rev. B **93**, 201104 (2016).
- [87] R. Singha, A. Pariari, B. Satpati, and P. Mandal, ArXiv e-prints (2016), 1602.01993.
- [88] X. Wang, X. Pan, M. Gao, J. Yu, J. Jiang, J. Zhang, H. Zuo, M. Zhang, Z. Wei, W. Niu, et al., ArXiv e-prints (2016), 1604.00108.
- [89] J. Hu, Z. Tang, J. Liu, X. Liu, Y. Zhu, D. Graf, Y. Shi, S. Che, C. N. Lau, J. Wei, et al., arXiv preprint arXiv:1604.06860 (2016).
- [90] Y. Wu, L.-L. Wang, E. Mun, D. D. Johnson, D. Mou, L. Huang, Y. Lee, S. L. Budko, P. C. Canfield, and A. Kaminski, ArXiv e-prints (2016), 1603.00934.
- [91] J. L. Lu, W. Luo, X. Y. Li, S. Q. Yang, J. X. Cao, X. G. Gong, and H. J. Xiang, ArXiv e-prints (2016), 1603.04596.
- [92] N. Goldman and J. Dalibard, Phys. Rev. X **4**, 031027 (2014).
- [93] A. G. Grushin, A. Gómez-León, and T. Neupert, Phys. Rev. Lett. **112**, 156801 (2014).
- [94] L. D'Alessio, ArXiv e-prints (2014), 1412.3481.
- [95] A. G. Grushin, A. Gómez-León, and T. Neupert, ArXiv e-prints (2015), 1503.02580.
- [96] H. B. Nielsen and M. Ninomiya, Nucl. Phys. B **185**, 20 (1981).
- [97] R. Nair, P. Blake, A. Grigorenko, K. Novoselov, T. Booth, T. Stauber, N. Peres, and A. Geim, Science **320**, 1308 (2008).
- [98] Y. Xu and C. Zhang, Phys. Rev. A **93**, 063606 (2016).
- [99] G. Jotzu, M. Messer, R. Desbuquois, M. Lebrat, T. Uehlinger, D. Greif, and T. Esslinger, Nature **515**, 237 (2014).
- [100] C. V. Parker, L.-C. Ha, and C. Chin, Nat. Phys. **9**, 769 (2013).
- [101] W. Zheng and H. Zhai, Phys. Rev. A **89**, 061603 (2014).
- [102] Y. T. Katan and D. Podolsky, Phys. Rev. Lett. **110**, 016802 (2013).
- [103] C.-K. Chan, Y.-T. Oh, J. H. Han, and P. A. Lee, ArXiv e-prints (2016), 1605.05696.
- [104] A. Narayan, ArXiv e-prints (2016), 1607.02503.
- [105] P. Hořava, Phys. Rev. Lett. **95**, 016405 (2005).
- [106] Y. X. Zhao and Z. D. Wang, Phys. Rev. Lett. **110**, 240404 (2013).
- [107] For a simple narrative, we do not distinguish between the terms “nodal line” and “nodal ring” hereafter.
- [108] In general, band touching is protected by the combination of topology and symmetry[105, 106].
- [109] The general incident angle is discussed in Supplemental Material.

Supplemental Material

This supplemental material contains: (i) The creation of Weyl points in nodal line semimetals by circularly polarized light with a general incident angle, (ii) The derivation of the anomalous Hall conductivity, and (iii) Details of experimental estimations.

CREATION OF FLOQUET WEYL POINTS BY INCIDENT LIGHT IN AN ARBITRARY DIRECTION

In the main text we have considered the case that the incident light is along the x direction, which is in the plane of nodal line. In this supplemental material we treat the cases of general incident angles. We shall see that the main results are qualitatively the same, except when the light is along the z direction, for which Floquet Weyl points cannot be created.

As the Hamiltonian has rotation symmetry in x - y plane, we can always rotate along the z axis so that the incident light is parallel to the $x - z$ plane. Let us denote the angle between the incident light and the x axis as θ (see Fig.4). The vector potential is

$$\mathbf{A}(t) = A_0(\sin\theta \sin(\omega t + \phi), \cos(\omega t), \cos\theta \sin(\omega t + \phi)), \quad (14)$$

where $\phi = 0$ and $\phi = \pi$ corresponds to right-handed and left-handed circularly polarized light, respectively. The time-periodic Hamiltonian can be expanded as $\mathcal{H}(\mathbf{k}, t) = \sum_n \mathcal{H}_n(\mathbf{k})e^{in\omega t}$, with the Fourier components

$$\begin{aligned} \mathcal{H}_0(\mathbf{k}) &= [m - Be^2A_0^2 - Bk^2]\tau_x + vk_z\tau_z, \\ \mathcal{H}_{\pm 1}(\mathbf{k}) &= -eA_0[B(k_y \mp ie^{\pm i\phi}k_x \sin\theta \mp ie^{\pm i\phi}k_z \cos\theta)\tau_x \\ &\quad \pm (ie^{\pm i\phi}v \cos\theta/2)\tau_z], \\ \mathcal{H}_{\pm 2}(\mathbf{k}) &= -Be^2A_0^2(1 - e^{\pm i2\phi})\tau_x/4. \end{aligned} \quad (15)$$

and $\mathcal{H}_n = 0$ for $|n| > 2$. The effective time-independent Hamiltonian can be obtained as

$$\begin{aligned} \mathcal{H}_{\text{eff}}(\mathbf{k}) &= \mathcal{H}_0 + \sum_{n \geq 1} \frac{[\mathcal{H}_{+n}, \mathcal{H}_{-n}]}{n\omega} + \mathcal{O}\left(\frac{1}{\omega^2}\right) \\ &= [m - Be^2A_0^2 - Bk^2]\tau_x + vk_z\tau_z + \lambda \cos\theta k_y \tau_y \end{aligned} \quad (16)$$

where $\lambda = -2Bve^2A_0^2 \cos\phi/\omega$. Therefore, tuning the incident direction from $\theta = 0$ (i.e. the x direction) to a general θ changes the y -th Fermi velocity of the Floquet Weyl points to $\lambda \cos\theta$. When $\cos\theta \neq 0$, i.e., the incident light is not in z direction, two Weyl points are created at $\mathbf{K}_{\pm} = (\pm \sqrt{\frac{m}{B} - e^2A_0^2}, 0, 0)$. Therefore, as long as the incident light is not perpendicular to the plane of nodal line/ring, the nodal line semimetal will be driven to Weyl semimetal by a circularly polarized light.

DEVIATION OF THE FORMULAS OF ANOMALOUS HALL CONDUCTIVITY

According to the Floquet theory(see e.g. Ref.[65]), the wavefunction $\Psi_{\alpha}(\mathbf{k}, t)$ that satisfies the time-dependent

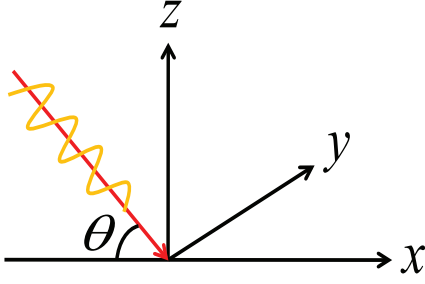


FIG. 4: Sketch of the incident angle.

Schrodinger equation $i\partial_t\Psi_\alpha(\mathbf{k}, t) = \mathcal{H}(\mathbf{k}, t)\Psi_\alpha(\mathbf{k}, t)$ can be written as $\Psi_\alpha(\mathbf{k}, t) = e^{-i\epsilon_\alpha t}\Phi_\alpha(\mathbf{k}, t)$, in which ϵ_α is the so-called quasi-energy and $\Phi_\alpha(\mathbf{k}, t)$ is periodic, namely, $\Phi_\alpha(\mathbf{k}, t + T) = \Phi_\alpha(\mathbf{k}, t)$, $T = 2\pi/\omega$ being the driven period. The periodic function $\Phi_\alpha(\mathbf{k}, t)$ satisfies $[\mathcal{H}(\mathbf{k}, t) - i\partial_t]\Phi_\alpha(\mathbf{k}, t) = \epsilon_\alpha\Phi_\alpha(\mathbf{k}, t)$.

Since $\Phi_\alpha(\mathbf{k}, t)$ is periodic, it can be expanded as $\Phi_\alpha(\mathbf{k}, t) = \sum_n e^{in\omega t}\Phi_\alpha^{(n)}(\mathbf{k})$, in which the Fourier components $\Phi_\alpha^{(n)}(\mathbf{k})$ satisfy the Floquet equation

$$[\epsilon_\alpha(k) - n\omega]\Phi_\alpha^{(n)}(\mathbf{k}) = \sum_m \mathcal{H}_{n-m}(\mathbf{k})\Phi_\alpha^{(m)}(\mathbf{k}) \quad (17)$$

with $\mathcal{H}_{n-m}(\mathbf{k}) = \frac{1}{T} \int_0^T dt e^{i(m-n)\omega t} \mathcal{H}(\mathbf{k}, t)$. In the off-resonant regime (ω much larger than other energy scale), based on perturbation theory[65], it is found that

$$\begin{aligned} \mathcal{H}_{\text{eff}}(\mathbf{k})\Phi_\alpha^{(0)}(\mathbf{k}) &= E_\alpha(\mathbf{k})\Phi_\alpha^{(0)}(\mathbf{k}), \\ \Phi_\alpha^{(n)}(\mathbf{k}) &= -\frac{\mathcal{H}_n}{n\omega}\Phi_\alpha^{(0)}(\mathbf{k}) \quad \text{for } n \neq 0. \end{aligned} \quad (18)$$

where

$$\mathcal{H}_{\text{eff}}(\mathbf{k}) = \mathcal{H}_0 + \sum_{n \geq 1} \frac{[\mathcal{H}_{+n}, \mathcal{H}_{-n}]}{n\omega} + O\left(\frac{1}{\omega^2}\right) \quad (19)$$

It follows from the linear response theory[66] that the formula for the Hall conductivity is given by

$$\sigma_{\mu\nu} = e^2 \epsilon_{\mu\nu\rho} \int \frac{d^3k}{(2\pi)^3} \sum_\alpha f_\alpha(k) [\nabla_{\mathbf{k}} \times \mathcal{A}_\alpha(\mathbf{k})]_\rho, \quad (20)$$

where $\mathcal{A}_\alpha(\mathbf{k}) = -i \ll \Phi_\alpha(\mathbf{k}) | \nabla_{\mathbf{k}} | \Phi_\alpha(\mathbf{k}) \gg \equiv \frac{1}{T} \int_0^T dt \langle \Phi_\alpha(\mathbf{k}, t) | \nabla_{\mathbf{k}} | \Phi_\alpha(\mathbf{k}, t) \rangle$. The Berry connection $\mathcal{A}_\alpha(\mathbf{k})$ can also be written as

$$\mathcal{A}_\alpha(\mathbf{k}) = \sum_n \mathcal{A}_{\alpha,n}(\mathbf{k}) = -i \sum_n \langle \Phi_\alpha^{(n)}(\mathbf{k}) | \nabla_{\mathbf{k}} | \Phi_\alpha^{(n)}(\mathbf{k}) \rangle \quad (21)$$

As has been obtained in the main text, $\mathcal{H}_{\text{eff}}(\mathbf{k})$ takes the following form,

$$\mathcal{H}_{\text{eff}}(\mathbf{k}) = [\tilde{m} - Bk^2]\tau_x + vk_z\tau_z + lk_y\tau_y. \quad (22)$$

It is readily found that $E_{\alpha=\pm}(\mathbf{k}) = \pm \sqrt{[\tilde{m} - Bk^2]^2 + v^2k_z^2 + l^2k_y^2}$, and $\Phi_\alpha^{(0)}(\mathbf{k})$ are given by

$$\Phi_+^{(0)}(\mathbf{k}) = \begin{pmatrix} \cos \frac{\theta_{\mathbf{k}}}{2} \\ \sin \frac{\theta_{\mathbf{k}}}{2} e^{i\varphi_{\mathbf{k}}} \end{pmatrix}, \Phi_-^{(0)}(\mathbf{k}) = \begin{pmatrix} \sin \frac{\theta_{\mathbf{k}}}{2} e^{-i\varphi_{\mathbf{k}}} \\ -\cos \frac{\theta_{\mathbf{k}}}{2} \end{pmatrix}, \quad (23)$$

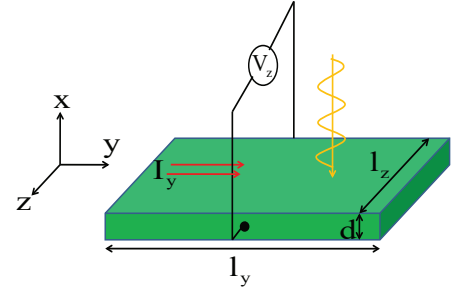


FIG. 5: Sketch of the experimental setup for the measurement of anomalous Hall effect. The nodal line lies in the x - y plane, and the circularly polarized light is incident along the x direction. I_y denotes an electric current in the y direction, l_y is the spacing between the current contacts, l_z is the spacing between the voltage contacts, d is the thickness of the sample, and V_z is the Hall voltage to be measured.

where $\theta_{\mathbf{k}} = \arccos \frac{vk_z}{E_+(\mathbf{k})}$ and $\varphi_{\mathbf{k}} = \arctan \frac{lk_y}{\tilde{m} - Bk^2}$. For the case that the occupation is close to equilibrium, namely, $f_{\pm,n}(k) = \delta_{n,0} n_{\pm}(E_{\pm}(\mathbf{k}))$, where $n_{\pm}(E_{\pm}(\mathbf{k})) = 1/(e^{(E_{\pm}(\mathbf{k}) - \mu)/T} + 1)$ is the Fermi-Dirac distribution. With the $O(1/\omega^2)$ terms omitted, the Hall conductivity takes the following form:

$$\sigma_{\mu\nu} = e^2 \epsilon_{\mu\nu\rho} \int \frac{d^3k}{(2\pi)^3} \sum_{i=\pm} n_i(E_i(\mathbf{k})) [\nabla_{\mathbf{k}} \times \mathcal{A}_{i,0}(\mathbf{k})]_\rho. \quad (24)$$

A combination of Eq.(21) and Eq.(23) gives

$$\mathcal{A}_{+,0}(\mathbf{k}) = -\mathcal{A}_{-,0}(\mathbf{k}) = \sin^2 \frac{\theta_{\mathbf{k}}}{2} \nabla_{\mathbf{k}} \varphi_{\mathbf{k}}, \quad (25)$$

thus Eq.(24) can be rewritten as

$$\sigma_{\mu\nu} = \frac{e^2}{2} \epsilon_{\mu\nu\rho} \int \frac{d^3k}{(2\pi)^3} \sin \theta_{\mathbf{k}} [\nabla_{\mathbf{k}} \theta_{\mathbf{k}} \times \nabla_{\mathbf{k}} \varphi_{\mathbf{k}}]_\rho (n_+ - n_-), \quad (26)$$

this formula can be further rewritten as

$$\sigma_{\mu\nu} = \frac{e^2}{2} \int \frac{d^3k}{(2\pi)^3} [\hat{\mathbf{d}} \cdot (\partial_{k_\mu} \hat{\mathbf{d}} \times \partial_{k_\nu} \hat{\mathbf{d}})] (n_+ - n_-), \quad (27)$$

where $\hat{\mathbf{d}} = (\sin \theta_{\mathbf{k}} \cos \varphi_{\mathbf{k}}, \sin \theta_{\mathbf{k}} \sin \varphi_{\mathbf{k}}, \cos \theta_{\mathbf{k}})$. The unit vector $\hat{\mathbf{d}}$ can also be expressed in the form $\hat{\mathbf{d}} \equiv \mathbf{d}/|\mathbf{d}|$ with $\mathbf{d} = \text{Tr}[\hat{\tau}^3 \mathcal{H}_{\text{eff}}]/2$. A direct calculation leads to the final expression

$$\sigma_{yz} = \frac{e^2}{2} \int \frac{dk^3}{(2\pi)^3} \frac{\lambda v (\tilde{m} - 2Bk_x^2 + Bk^2)}{[E_+(k)]^3} (n_+ - n_-). \quad (28)$$

DETAILS OF EXPERIMENTAL ESTIMATIONS

In this section, we provide more details for the estimated transport measurements discussed in the main text. We still assume that the nodal line lies in the x - y plane, and the circularly polarized light is incident along the x direction. A sketch of the experimental setup for measurement of the anomalous Hall effect is given in Fig.5. In this setup, I_y is a constant

current in the y direction, l_y is the spacing between current contacts and l_z is the spacing between voltage contacts, d is the thickness of the sample, and V_z refers to the Hall voltage to be measured. Assuming a uniform distribution of the current through the entire thickness, we obtain the Hall voltage V_z as follows [84]:

$$V_z \approx \frac{\sigma_{yz}\delta/d}{\sigma_{yy}^2 + (\sigma_{yz}\delta/d)^2} \times \frac{l_z}{l_y d} \times I_y, \quad (29)$$

where δ is the penetration depth of light, given by $\delta(\omega) = \frac{n(\omega)\epsilon_0 c}{\text{Re}\sigma_{xx}(\omega)}$, where $n(\omega)$ is the refraction index of the sample, ϵ_0 the permittivity of vacuum, c the speed of light, and $\text{Re}\sigma_{xx}(\omega)$ denotes the real part of the optical conductivity in the x direction. For nodal line semimetal, if we assume that the Fermi velocities in the two transverse directions are the same, we have $\text{Re}\sigma_{xx}(\omega) = \frac{e^2}{h} \frac{\pi}{8} \sqrt{\frac{m}{B}}$.

In the following, we take the experimentally-confirmed nodal line semimetal ZrSiS as a concrete example to estimate the Hall conductivity σ_{yz} and the Hall voltage V_z . For a circularly polarized light parallel to the x - y plane (or the ab plane) of ZrSiS, the distance between induced Weyl points is $\Delta \approx 2\pi/a$ (i.e. the size of the nodal line in ZrSiS is very large)

with $a \approx 3.5\text{\AA}$ the lattice constant in x - y plane. Thus

$$\sigma_{yz} = \frac{e^2}{h} \frac{\Delta}{2\pi} \approx 1.0 \times 10^5 \Omega^{-1} m^{-1}. \quad (30)$$

To be close to the experimental condition[78], we take the frequency of light to be $\hbar\omega = 120$ meV. Let us take the refraction index to be $n(\omega) \approx 3$, then the penetration depth is[84]

$$\begin{aligned} \delta &\approx \frac{n(\omega)\epsilon_0 c}{(\pi e^2/16h)\Delta} \\ &\approx \frac{3 \times 8.85 \times 10^{-12} \times 3 \times 10^8}{\left(\frac{1.6^2 \times 10^{-38}}{6.63 \times 10^{-34}}\right) \times (3.14^2/8)} a \\ &\approx 167a \approx 586\text{\AA}. \end{aligned} \quad (31)$$

We shall use the measured value[87] of the dc conductivity σ_{xx} at 300 K, which is $\sigma_{xx} \approx 6.6 \times 10^6 \Omega^{-1} m^{-1}$. Let us take the sample size to be $l_y = l_z = 100 \mu\text{m}$, $d = 100$ nm. Suppose that the electric current is $I_y = 100$ mA, then a combination of Eq.(29), Eq.(30) and Eq.(31) yields the resultant Hall voltage $V_z \approx 1.3$ mV, which is easily observable in realistic experiments.